ASSESSING BRIGHTNESS TEMPERATURE SENSITIVITY TO AEROSOLS IN THE MARTIAN ATMOSPHERE USING THE ENSEMBLE MARS ATMOSPHERE REANALYSIS SYSTEM (EMARS)

R. P. McMichael, *Department of Meteorology and Atmospheric Science, The Pennsylvania State University, University Park, PA, USA (rpm5826@psu.edu)*, **S. J. Greybush**, *Department of Meteorology and Atmospheric Science, The Pennsylvania State University, University Park, PA, USA*, **R. J. Wilson**, *Space Science and Astrobiology Division, NASA Ames Research Center, Moffett Field, CA, USA*.

Introduction:

The Ensemble Mars Atmosphere Reanalysis System (EMARS; Greybush et al., 2019a) assimilates retrievals from the Thermal Emission Spectrometer (TES; Smith et al., 2001) and Mars Climate Sounder (MCS; Kleinböhl et al., 2009) instruments into the Geophysical Fluid Dynamics Laboratory Mars Global Climate Model (GFDL/NASA MGCM) using the Local Ensemble Transform Kalman Filter (LETKF; Hunt et al., 2007). One of the primary science objectives of EMARS is to better model and understand global dust storms, in particular characterizing which atmospheric states lead to their initiation and how these storms evolve. Of particular importance to this objective is determining what modeling and assimilation techniques and observing system design is the most helpful for constraining aerosols, estimating dust lifting, and improving dust storm forecasting. Hinson (2006) suggests that dust storm genesis is linked to baroclinic wave activity in the northern midlatitudes. For EMARS to investigate dust storm genesis, conditions in the lower atmosphere (pressures exceeding 350 Pa, the altitudes associated with peak baroclinic wave activity) need to be well-characterized. Unfortunately, at the times of year, latitudes, and altitudes associated with baroclinic wave activity, the success rate of MCS retrievals falls off precipitously (Hinson and Wilson, 2021). When reanalysis uses these MCS temperature retrievals, the 16-member ensemble does not always converge to a unique synoptic state (Greybush et al., 2019b; Battallio, 2022), compromising the integrity of model output. This indicates that the information contained in MCS retrievals needs to be used in conjunction with additional data to support a comprehensive investigation of near-surface wave activity, and in turn dust storm initiation. EMARS currently assimilates atmospheric temperature retrievals to update atmospheric temperatures, winds, and surface pressures, and updates dust via the Montabone et al. (2015) dust scenarios, which incorporate MCS dust retrievals. To meet the EMARS science objectives, we turn to MCS brightness temperature observations, which are likely impacted by surface temperatures, lower atmospheric temperatures, and aerosols (Hinson and Wilson, 2021). Therefore, the next version of EMARS plans to use brightness temperature observations to update the atmospheric temperature and dust fields. This work picks up where Wilson et al. (2011) left off. Before full assimilation is implemented, we need to quantify the correlation between brightness temperatures and model fields (e.g., temperature, dust, water ice, surface properties). To do this, experiments have been performed with model output 23-μm and 32-μm brightness temperatures (T_{23} and T_{32}), corresponding to the TES and B1 MCS observation channels sensitive to dust (Christensen et al., 2001; McCleese et al., 2007). The primary question these experiments are hoping to answer is whether the transient eddies observed in brightness temperatures (Hinson and Wilson, 2021) are the result of surface temperature fluctuations, near-surface air temperature fluctuations, or dust being carried by transient eddies.

Multiple Linear Regression Model:

Experimental Setup: A multiple linear regression model was built to recreate T_{23} time series from various physical fields within EMARS. The primary goal of this portion of the project was not to create a data-driven forward model that accurately predicts brightness temperatures but rather to understand what model variables the brightness temperatures are most sensitive to at this wavelength. The version of the model shown here utilized surface temperature, column dust opacity, column water ice, and surface carbon dioxide and water ices as predictors, such that T_{23} was the predictand. The statistical model was trained using predictor and predictand data from EMARS reanalysis output between MY 28 L_S 111º and MY 29 L_S 125º. This model was then verified against EMARS reanalysis predictand data spanning MY 29-33. The model was tested at tropical (2.57º S) and midlatitude (43.7º N) locations, all hours of the day, and four times of year – 30º areocentric longitude (L_s) chunks starting at the solstices and equinoxes. During model training, regression coefficients constraining the relationships between T_{23} and the physical predictors were calculated.

Results: The relationship between T_{23} and column dust opacity is illustrated in Figure 1. During the day, elevated dust levels correspond to decreased T_{23}, whereas at night, elevated dust levels correspond to increased T_{23}. This suggests that airborne dust is absorbing and re-emitting upwelling longwave radiation at night and reflecting incident shortwave radiation

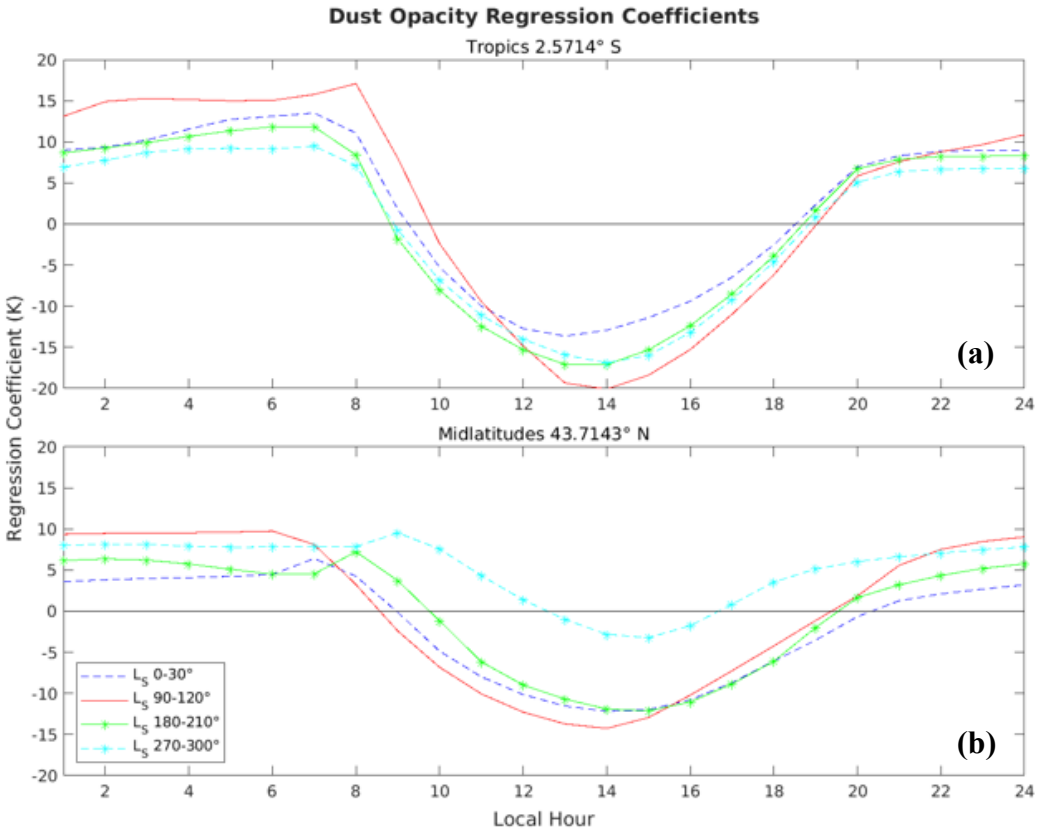

Figure 1: Diurnal evolution of column dust opacity regression coefficient at (a) 2.5714 ºS and (b) 43.7143 ºN for the northern vernal equinox (dashed blue), summer solstice (red), autumnal equinox (green), and winter solstice (dashed cyan) seasons, where each season is represented by a 30º areocentric longitude period starting at the respective date. Asterisks denote seasons with higher dust opacity (L_S 180-210º, 270-300º). Positive values indicate column dust opacity is positively correlated with T_{23}, where negative values indicate negative correlation.

during the day. The impact of this greenhouse effect varies by latitude and time of year, for instance becoming significantly weaker during the northern midlatitude winter. There is also a significant positive correlation between surface temperature and brightness temperature (not pictured), expected since the brightness temperature mirrors the surface temperature in clear-sky conditions. Since T_{23} is sensitive to both dust and surface emission, it stands to reason that the height at which dust is present (and corresponding atmospheric temperature) could also have a significant impact on the observed brightness temperature. Constraining brightness temperature behavior by column variables alone is a good starting point, but a comprehensive picture requires altitude-dependent temperature and dust fields as well.

Ensemble Sensitivity Analysis:

Experimental Setup: One of the significant impacts on the diurnal variability of brightness temperature is airborne dust, which serves to reduce the diurnal temperature range (as shown in Figure 1). To further quantify the impact of airborne dust, we wanted to assess whether airborne dust drives a greenhouse or anti-greenhouse effect. To examine the impact of dust, we examined the relative impacts between ensemble members with different dust forcing. The 16 ensemble members in EMARS vary as a function of both dust and water ice forcing, enabling the model to account for some of the uncertainties associated with aerosol particle size distributions and composition (Greybush et al., 2019a). Using individual ensemble members enables us to visualize different potential atmospheric scenarios based on varying physical assumptions and improve our best estimate from this more detailed examination. The dust forcing tuning parameter in EMARS is a scaling factor applied when converting the dust mass mixing ratio to opacity, which is adjusted such that the dust opacity increases uniformly from 0.7 to 1.3 times the amount of the average ensemble member. This ensemble comparison currently examines the members with the strongest and weakest dust radiative forcing but also identical water ice forcing to isolate the aerosol impacts of dust. T_{32} was taken from these members from EMARS free run data, reflecting the behavior of the MGCM without the influence of assimilated temperatures to better determine the model relationship between atmospheric dust, surface temperature, and brightness

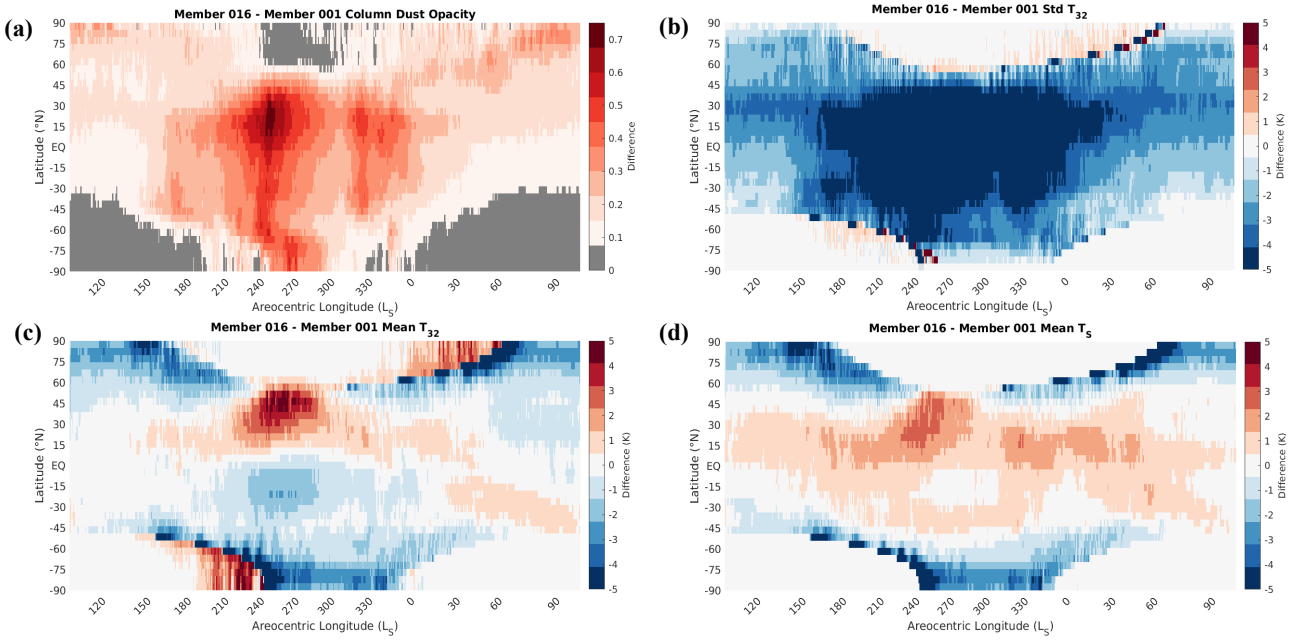

Figure 2: The seasonal evolution of the difference between zonally-averaged (a) column dust opacity, (b) T_{32} standard deviation, (c) T_{32}, and (d) surface temperature between the EMARS ensemble members with highest and lowest dust radiative forcing. The areas with little to no shading at the highest latitudes correspond to the polar ice caps, and areas with bright shading near these edges correspond to differences driven by varying locations of the ice cap edge between ensemble members.

temperature. This not only provides a clearer picture of how brightness temperature is currently impacted by other model variables, but also provides a framework for how dust and temperature could be updated by brightness temperature during ensemble data assimilation. From this point, brightness temperatures were evaluated across a latitude circle at a given time from MY 30 L_S 101.42º to MY 31 L_S 105.75º. Zonally-averaged brightness temperature was taken to reflect the mean and used to assess whether dust was heating or cooling the atmosphere at a given latitude. The standard deviation of brightness temperature was taken across the same latitude circle. Since all this data was taken from the same standard time, and not local time, these brightness temperatures span the full diurnal cycle. The standard deviation is used here as a metric to evaluate changes to magnitude of the diurnal cycle. In comparing the relative impacts of dust forcing, we compared the dustiest conditions (member 16) to the clearest conditions (member 1). This includes comparison of the column dust opacity, as well as the mean and standard deviation (as defined above) of T_{32} and surface temperature.

Results: The horizontal and temporal dust distribution within EMARS is derived from the Mars Climate Database version 5 gridded dust scenarios (Montabone et al., 2015). As expected, the dustiest times of year are shortly before and after the winter solstice. Since this is the time of year with the highest column dust opacities, this is also the time of year where the relative difference between ensemble members 16 and 1 is most noticeable (Figure 2a). As expected from the results of the regression model, the times of year and latitudes associated with the largest departure in dust opacity is aligned with the times of year and latitudes associated with the largest reduction in diurnal brightness temperature standard deviation (Figure 2b). The mean brightness temperature is not uniformly increased or decreased, but rather varies with respect to the location of the subsolar point (Figure 2c). One of the physical mechanisms likely driving this T_{32} behavior is as follows. In the summertime hemisphere, enhanced dust reflects the ample incident shortwave radiation, reducing the total energy in the system. In the wintertime hemisphere, enhanced dust absorbs and re-emits upwelling longwave radiation, preventing energy from leaving the system. Additional support for this physical mechanism driving the model brightness temperature behavior can be in the seasonal evolution of surface temperature (Figure 2d), where the wintertime surface temperatures are elevated in dusty conditions. There are significant departures in the surface temperature and T_{32} behavior in the summertime hemisphere, indicating the importance of additional variables to T_{32} behavior.

As indicated earlier, brightness temperatures are highly dependent on the vertical temperature and dust profiles. For the vertical dust profile, the model equations for the lowest model level include a source and sink term for dust that relaxes the model column opacity towards the observations. Otherwise, three dust tracers are advected by model winds such that the

vertical profile is driven by advection and sedimentation (Greybush et al., 2019a). While the dust forcing tuning knob neatly increases the column dust opacity value between ensemble members, dust tracer mass mixing ratios do not uniformly increase in turn, likely due to the impact of dust radiative forcing on the model winds that scatter these tracers. More detailed analysis relating the vertical profiles of dust and air temperature to brightness temperature using EMARS free run data is forthcoming. . In particular, ensemble sensitivity analysis (especially across the full ensemble of 16 members) can inform how brightness temperature is related to atmospheric temperatures and dust at particular vertical levels. These ensemble correlations are then used by the data assimilation system to update the atmospheric state based on these observations. This study paves the way for use of actual MCS atmospheric brightness temperatures, along with MCS retrievals, for the next version of EMARS.

Acknowledgments:

We thank Hartzel Gillespie and Noah Polek-Davis for facilitating access to data from EMARS and consultation regarding its use and interpretation. We are grateful to Dave Hinson for insights on MCS brightness temperatures, and to the MCS team for their guidance on the dataset. This research was supported by the NASA Mars Data Analysis Program Grant 80NSSC20K1054. EMARS data utilized in this paper are available from the Penn State Data Commons at https://doi.org/10.18113/d3w375 (Greybush et al., 2019).

References:

Battalio, J. M., Transient Eddy Kinetic Energetics on Mars in Three Reanalysis Datasets, *J. Atmos. Sci.*, *79*(2), 361-382, 2022.

Christensen, P. R. et al., Mars Global Surveyor Thermal Emission Spectrometer experiment: Investigation description and surface science results, *J. Geophys. Res.*, *106*(E10), 23823, 2001.

Greybush, S. J., et al., The Ensemble Mars Atmosphere Reanalysis System (EMARS) Version 1.0, *Geosci. Data J.*, *6*(2), 137–150, 2019.

Greybush, S. J., H. E. Gillespie, and R. J. Wilson, Transient eddies in the TES/MCS Ensemble Mars Atmosphere Reanalysis System (EMARS), *Icarus*, *217*, 158-181, 2019.

Hinson, D. P., Radio occultation measurements of transient eddies in the northern hemisphere of Mars, *J. Geophys. Res. Planets*, *111*(E5), 2006.

Hinson, D. P. and R. J. Wilson, Baroclinic waves in the northern hemisphere of Mars as observed by the MRO Mars Climate Sounder and the MGS Thermal Emission Spectrometer, *Icarus*, *357*, 114-152, 2021.

Hunt, B. R., et al., Efficient data assimilation for Spatiotemporal Chaos: A local ensemble transform Kalman filter, *Phys. D: Nonlinear Phenom.*, *230*(1-2), 112-126, 2007.

Kleinböhl, A. et al., Mars Climate Sounder limb profile retrieval of atmospheric temperature, pressure, and dust and water ice opacity, *J. Geophys. Res. Planets, 114*(E10), 2009.

McCleese, D. J. et al., Mars Climate Sounder: An investigation of thermal and water vapor structure, dust and condensate distributions in the atmosphere, and energy balance of the polar regions, *J. Geophys. Res., 112*(E5), 2007.

Montabone, L., et al., Eight-year climatology of dust optical depth on Mars, *Icarus*, *251*, 65-95, 2015.

Smith, M. D., et al., One Martian year of atmospheric observations by the thermal emission spectrometer, *Geophys. Res. Lett.*, *28*(22), 4263-4266, 2001.

Wilson, R. J., J. Noble, and S. J. Greybush, The Derivation of Atmospheric Opacity from Surface Temperature Observations, *Mars Atmosphere Modeling and Observations*, *4th*, 2011.